IVYSPRING INTERNATIONAL PUBLISHER

Theranostics

2017; 7(5): 1047-1061. doi: 10.7150/thno.18099

Research Paper

A Unique Recombinant Fluoroprobe Targeting Activated Platelets Allows *In Vivo* Detection of Arterial Thrombosis and Pulmonary Embolism Using a Novel Three-Dimensional Fluorescence Emission Computed Tomography (FLECT) Technology

Bock Lim[1]✉, Yu Yao[1], Alex Lin-i Huang[1,3], May Lin Yap[1,5], Ulrike Flierl[1,2], Jathushan Palasubramaniam[1], Maria T.K. Zaldivia[1,3], Xiaowei Wang[1,3], Karlheinz Peter[1,3,4]✉

1. Atherothrombosis & Vascular Biology, Baker IDI Heart and Diabetes Institute, Melbourne, Australia.
2. Department of Cardiology, Medizinische Hochschule, Hanover, Germany.
3. Department of Medicine Monash University, Melbourne, Australia;
4. Department of Immunology, Monash University, Melbourne, Australia;
5. Department of Pathology, University of Melbourne, Melbourne, Australia.

✉ Corresponding authors: Dr Bock Lim & Prof Karlheinz Peter, Atherothrombosis & Vascular Biology, Baker IDI Heart and Diabetes Institute, 75 Commercial Road, Melbourne, Victoria 3004, Australia Fax: +61(0)385321100, Tel: +61(0)385321495 Email: Bock.Lim@bakeridi.edu.au; Karlheinz.Peter@bakeridi.edu.au.

Received: 2016.10.26; Accepted: 2017.01.17; Published: 2017.02.26

Abstract

Progress in pharmaceutical development is highly-dependent on preclinical *in vivo* animal studies. Small animal imaging is invaluable for the identification of new disease markers and the evaluation of drug efficacy. Here, we report for the first time the use of a three-dimensional fluorescence bioimager called FLuorescence Emission Computed Tomography (FLECT) for the detection of a novel recombinant fluoroprobe that is safe, easily prepared on a large scale and stably stored prior to scan. This novel fluoroprobe (Targ-Cy7) comprises a single-chain antibody-fragment ($scFv_{Targ}$), which binds exclusively to activated-platelets, conjugated to a near-infrared (NIR) dye, Cy7, for detection. Upon mouse carotid artery injury, the injected fluoroprobe circulates and binds within the platelet-rich thrombus. This specific *in vivo* binding of the fluoroprobe to the thrombus, compared to its non-targeting control-fluoroprobe, is detected by the FLECT imager. The analyzed FLECT image quantifies the NIR signal and localizes it to the site of vascular injury. The detected fluorescence is further verified using a two-dimensional IVIS® Lumina scanner, where significant NIR fluorescence is detected *in vivo* at the thrombotic site, and *ex vivo*, at the injured carotid artery. Furthermore, fluorescence levels in various organs have also been quantified for biodistribution, with the highest fluoroprobe uptake shown to be in the injured artery. Subsequently, this live animal imaging technique is successfully employed to monitor the response of the induced thrombus to treatment over time. This demonstrates the potential of using longitudinal FLECT scanning to examine the efficacy of candidate drugs in preclinical settings. Besides intravascular thrombosis, we have shown that this non-invasive FLECT-imaging can also detect *in vivo* pulmonary embolism. Overall, this report describes a novel fluorescence-based preclinical imaging modality that uses an easy-to-prepare and non-radioactive recombinant fluoroprobe. This represents a unique tool to study mechanisms of thromboembolic diseases and it will strongly facilitate the *in vivo* testing of antithrombotic drugs. Furthermore, the non-radiation nature, low-cost, high sensitivity, and the rapid advancement of optical scanning technologies make this fluorescence imaging an attractive development for future clinical applications.

Key words: FLuorescence Emission Computed Tomography, near-infrared, single-chain antibody, activated-platelets, fluoroprobe, thrombosis and embolism.

Introduction

Preclinical testing involving small animal studies are fundamental to the development of new pharmaceutical products. Targeted molecular imaging that characterizes and measures biological processes in these animals at cellular, molecular and whole body levels has proven to be highly valuable. In this process, researchers commonly employ small animal bioimaging technologies to study *in vivo* activities and localization of the candidate of interest as a prerequisite for its clinical translation. A variety of imaging modalities including optical, nuclear, magnetic resonance (MRI) and sonographic imaging are available, with their respective advantages and limitations. Of note, optical imaging is sensitive, versatile and radiation-free. With advances in optical technology and fluorescence probe design, this modality is gaining major impetus in preclinical imaging.

Optical imaging is used in both basic science laboratories and clinical practice [1, 2]. With many innovations, this imaging modality has evolved from basic light microscopy to sophisticated fluorescence techniques that allow targeted imaging of biological processes within the living body. *In vivo* fluorescence imaging requires the use of probes that can absorb (excitation) and emit (emission) light at specific wavelengths. Factors influencing the excitation and emission of a probe should be considered for its use in an *in vivo* setting. Many biological components like sugar, fatty acids, amino acids, water, ions, DNA, RNA, cell membrane and organelles can absorb the incoming excitation light and limit its depth of penetration to reach the *in vivo* target. Besides absorption, many tissues have endogenous auto-fluorescent properties that can mask signals from the probe. These two issues can be overcome by the use of Near-Infrared (NIR) probes, as most natural absorbers and emitters do not possess fluorescent properties of such high wavelength spectrum (700 nm – 1000 nm). Hence imaging at this spectral range provides a crucial "optical window" for researchers, and has encouraged the development of different NIR probes. Cyanine dyes are an excellent member of the NIR probe family as they have good photostability, high molar absorptivity and strong fluorescence emission [3, 4]. Well studied cyanine dyes used in many *in vitro* and *ex vivo* immunofluorescence microscopy include Cy5.5 (ex: 673 nm, em: 707 nm), Cy7 (ex: 750 nm, em: 773 nm) and Indocyanine Green (ICG; ex: 780 nm, em: 830 nm), with the latter already approved for clinical use. These dyes can be conjugated to proteins/antibodies of interest to produce targeted recombinant fluoroprobes that bind to, and thus track, protein/cells of interest in different animal models. This is important in the identification of new biomarkers and evaluation of candidate drugs, as their *in vivo* properties may shed light on their clinical relevance and application. *In vivo* imaging has been made possible by recent advances in imaging equipment, through the development of highly sensitive detectors and novel filters, sophisticated mathematical computations and powerful analytical software, the many unfavorable imaging photo-properties within biological tissues such as photon scattering and light attenuation, can now be avoided or compensated. Examples of such NIR scanners include Optix MX3, IVIS and the FMT. Recently, a world-first true 360 degree tomographic system termed InSyTe FLECT (TriFoil Imaging, USA) scanner was developed with the ability to achieve homogeneous sensitivity, uniform resolution and accurate quantification of fluoroprobes throughout the subject. Here we report for the first time the use of this three-dimensional optical imager to detect thrombi via a newly developed fluorescence fluoroprobe that targets activated-platelets.

Platelets are the most abundant cells in the circulation, promoting hemostasis to maintain vasculature integrity. In recent years, their role in inflammatory processes such as autoimmunity and atherosclerosis has also been well described [5-7]. In atherothrombosis, activated-platelets are associated with the inflammatory process that drives vulnerability of atherosclerotic plaques [8-10]. In addition, platelets are critical in thrombotic vascular occlusion, the underlying pathology of catastrophic events such as myocardial infarction, pulmonary embolism and stroke. Collectively, thrombosis-related diseases are the leading causes of mortality and morbidity worldwide [11]. At present, clinical diagnosis of coronary diseases relies on coronary angiography. It merely provides information on the degree of luminal obstruction, but fails to inform the characteristics and stability of atherosclerotic plaques. We propose that targeting activated-platelets is an excellent strategy in the diagnosis of these diseases, and we have demonstrated their *in vivo* detection in an experimental mouse model of thrombosis using Positron Emission Tomography (PET) [12].

The targeting of activated-platelets for *in vivo* imaging can be achieved with a unique single-chain (scFv) antibody fragment specific for the glycoprotein IIb/IIIa receptor (GPIIb/IIIa), found in abundance on the platelet surface. This scFv ($scFv_{GPIIb/IIIa}$, termed

$scFv_{Targ}$ in this report) exclusively binds a site on GPIIb/IIIa that is only exposed upon platelet activation. Besides its specificity for activated-platelets, the single-chain is a small molecule (~33 kDa), thus has faster circulation clearance and can penetrate tissues more deeply, when compared to a complete antibody molecule (IgG: ~150 kDa). Consequently, it provides a better signal to background noise ratio and better access to target protein/cells. We have previously employed this scFv in various molecular imaging modalities such as intravital microscopy [13], ultrasound [14], PET [12] and MRI [15-18] of small animals. In these *in vivo* studies, no inhibitions of platelet aggregation, or bleeding prolongation or complications were observed with the dose used of the anti-activated-GPIIb/IIIa scFv.

In this study, we describe the generation of an activated-platelet targeting NIR fluoroprobe based on this scFv. This novel fluoroprobe will be verified *in vitro* and then used for the first time in *in vivo* FLECT-scanning, demonstrating potential utility of the scFvs and the FLECT technology for the detection and monitoring of thrombosis and thromboembolism.

Materials and Methods

Generation, production and purification of $scFv_{Targ}$-LPETGG and $scFv_{Mut}$-LPETGG

The cloning and production methods of both $scFv_{Targ}$-LPETGG and $scFv_{Mut}$-LPETGG (control) have been previously described [14, 19]. Here, a mammalian expression system for large-scale scFv production was employed using polyethylenimine (PEI) (Polyscience Inc., Germany)-transfection of human endothelial kidney cells (HEK293F) with a cloned DNA plasmid using the pSectag2A vector. At the time of transfection, HEK293F cells in Freestyle 293 expression medium (Invitrogen, USA) were at a cell density of $2x10^6$ cells/mL with viability greater than 95 %. Next, DNA plasmid (1 µg/mL) and PEI (3 µg/mL) at a 1:4 ratio was prepared and added at a 9:1 ratio of cell culture to DNA/PEI preparation. Cell culture medium was supplemented with 6 g/L glucose and 5 g/L lupin, and incubated at 37 °C, 5 % CO_2 with constant shaking at 110 rpm. At days 3, 5 and 7 post transfection, the culture medium was supplemented with 2 mM L-glutamine and glucose levels were maintained between 5–6 g/L. Following transfection, cell cultures were centrifuged at 3,000 g for 15 minutes at 4 °C and supernatant was collected for protein purification. The supernatant was dialysed against Phosphate Buffered Solution (PBS) overnight at 4 °C and purified by chromatography using an anti-His tag Ni column (5 mL bed volume). Final preparations were obtained by dialysis against PBS overnight at 4 °C and stored at -80 °C till use.

Production and purification of Sortase An enzyme

Sortase A, transpeptidase from *Staphylococcus aureus*, was produced using established protocol [19]. Briefly, Sortase A conceding plasmid was transformed into BL21-DE3 *E.coli* (Invitrogen). During production, transformed bacteria was cultured and allowed to reach an OD600 of 0.7 before IPTG at 1 mmol/L was added to induce sortase expression for 3 hours at 37°C. Sortase protein was then purified by chromatography using an anti-His tag Ni column as described above for scFvs.

Sortase enzymatic reaction for BCN-Targ/ BCN-Mut production

Bacterial transpeptidase enzyme, Sortase A, was used to bioconjugate $scFv_{Targ}$-LPETGG and $scFv_{Mut}$-LPETGG to the glycine residue on the N-terminal of cyclooctyne compound, BCN (bicyclo [6.1.0] non-4-yne). The sortase reaction was performed at a molar ratio of 1 scFv : 3 BCN : 3 Sortase A, in a buffered solution with 50 mM Tris, 150 mM NaCl, 0.5 mM $CaCl_2$ of pH 8.0, for 5 hours at 37 °C. The sortase reaction cleaved the His-tag from the scFv resulting in the generation of BCN-Targ or BCN-Mut. The reaction was purified using anti-His tag Ni column to remove free sortase enzyme and excess unconjugated scFv. The flow-through with the conjugated products was then dialysed against PBS overnight at 4 °C. The efficiency of the coupling procedure was analysed by SDS-PAGE and protein assay (BCA).

Azide-alkyne cycloaddition click-chemistry reaction

To generate the FLECT fluoroprobe, previously described click-chemistry [20] was used to conjugate BCN-Targ or BCN-Mut with Cy7 dye (Ex: 750 nm and Em: 773 nm) or Cy5 dye (for supplementary data; Ex: 649 nm and Em: 666 nm) carrying an azide functional group at a molar ratio of 1:2 respectively. The reaction was performed in PBS, pH 7 for 2 hours, at room temperature in an oxygen-free environment. Excess free dye was then removed by ultra-15 centrifugal filter unit (MWCO 10 kDa; Amicon, USA) before overnight dialysis against PBS buffer. Gel electrophoresis was performed to analyse the newly generated fluoroprobe and near infrared imaging (700 nm/800 nm) of the gel using the Odyssey Infrared Imaging System (LI-COR Biosciences) to confirm dye conjugation against the correct band size.

FLECT fluoroprobe *in vitro* analysis

Thrombus binding

Fresh citrated blood from healthy volunteers was centrifuged at 180 g for 10 minutes to obtain platelet-rich plasma (PRP). Every mL of PRP was added 5 µL of tissue thrompolastin, thromborel S (Dade Behring) and 25µL of 1M $CaCl_2$ for 15 minutes at 37 ^oC to induce thrombus formation. Thrombi were then incubated with either 2 µg/mL of Targ-Cy7 or Mut-Cy7 in 1 mL of PBS for an hour at room temperature with gentle mixing. The thrombi were then washed five times with PBS to remove unbound fluoroprobe. The fluorescence intensities of the thrombi were analysed using the Odyssey® CLx Infrared Imaging System (700 nm/800 nm; LI-COR Biotechnology, USA).

Activated-platelet binding

Fresh citrated blood from healthy mice was centrifuged at 180 g for 10 minutes to obtain PRP. Isolated resting platelets were prepared from the PRP by centrifugation (500 g, 10 minutes) in the presence of ACD (acid citrate dextrose) buffer, 0.05 µM prostaglandin E1 (PGE_1) and 0.01 U/mL apyrase twice. The final platelet pellet was resuspended in Tyrode's buffer (137 mmol/L NaCl, 2.68 mmol/L KCl, 11 mmol/L $NaHCO_3$, 10 mM Hepes, 0.42 mM NaH_2PO_4, 5 mM D-Glucose; pH 7.4) in the same volume as initial PRP and substituted with 1mM $MgCl_2$ and 2mM $CaCl_2$ final concentration. Either fluoroprobe at 5 µg/mL was added to the resting platelet suspension or activated-platelet suspension with 10 µM adenosine diphosphate (ADP). After 20 minutes of incubation at 37^oC, platelet suspension was fixed with 5 % paraformaldehyde, centrifuged and washed 5 times with PBS before blotted on filter paper and imaged on the Odyssey scanner (700 nm/ 800 nm).

GPIIb/IIIa-transfected Chinese Hamster Ovary (CHO) cells binding

CHO wild-type (WT) cells, or transfected CHO cells expressing either resting or activated GPIIb/IIIa [21] were used to ascertain the specific binding of the fluoroprobe to the activated integrin receptor. Briefly, 1 million cells of each cell-type were added with either Targ-Cy or Mut-Cy7 probes at 5 µg/mL and incubated for 20 minutes at 37^oC. Cells were then fixed, washed, blotted on filter paper and imaged on the Odyssey scanner as described above.

Animal models

Female athymic nude mice (15–20 g) were used in this study and were purchased from the Animal Resources Centre (WA, Australia). Animals were maintained at all times on a 12 hour light/dark cycle in a specific pathogen free environment and were supplied with food and water *ad libitum*. All animal studies were conducted in accordance with protocols approved by the Alfred Medical Research Education Precinct Animal Ethics Committee and the Monash University Animal Ethics Committee (Ethics Approval: E/1391/2013/B).

Ferric chloride carotid artery injury

This is a well described model of thrombosis [19, 22, 23]. Briefly, the left common carotid artery of an anesthetized mouse was dissected from circumferential connective tissues, and a 1 mm by 2 mm filter paper saturated with 5 % ferric chloride was placed under the artery for 3 minutes to induce vascular injury resulting in non-occlusive thrombus formation. After which FLECT fluoroprobe (Targ-Cy7 or Mut-Cy7) at 1 µg/g of body-weight was then intravenously (i.v.) injected into the animal and circulated for 45 minutes before FLECT/CT scanning.

Combined urokinase/integrilin treatment was performed on ferric chloride injured animals upon the completion of the first round of FLECT/CT scans. Here, mice were treated with a bolus intravenous injection of 500 Units/Kg and 200 µg/Kg of combined anti-thrombotic drugs, urokinase (Medac GmbH, UK) and integrilin (Schering-Plough Pty Limited, Australia) respectively, or same volume of PBS as control, and followed by infusion of the same drugs at 50 Units/Kg/minute and 20 µg/Kg/minute respectively or PBS for 20 minutes before the animals were rescanned to determine the efficacy of this therapy.

Pulmonary embolism

This pulmonary embolism model is based on a previously described method [24]. Here, anesthetized mouse received thromborel S (120 µg i.v., single dose) to induce circulatory thrombosis resulting in thrombi that migrated and lodged in the lungs. Upon observable changes to the breathing pattern of the mouse, suggesting pulmonary embolism, FLECT fluoroprobe (Targ-Cy7 or Mut-Cy7) at 1 µg/g of body-weight was i.v. injected and circulated for 45 minutes before FLECT/CT scanning. To verify that the detected FLECT/CT signals localized to the lungs, CT-contrast agent, Iopromide (Ultravist; Bayer, UK) was perfused into the lungs via the trachea following euthanasia. Mice were then rescanned on the FLECT/CT imager.

Post-scan, mice were euthanized and various tissues/organs were collected for *ex vivo* fluorescence scanning using the infrared IVIS® Lumina (Perkin Elmer, USA) imager to confirm and quantify the

detected fluorescence signal and histological analysis.

Near infrared animal imaging using FLECT/CT and IVIS® Lumina scanners

FLECT/CT

FLECT imaging was performed using the Trifoil InSyTe FLECT® imager (beta version; TriFoil Imaging, USA) with acquisition laser of 730 nm and filter of 803 nm wide. Surface, absorption and emission data was collected at 29 slices with 1mm spacing and 29 source angles/slice. Reconstruction analysis of FLECT image was at 1 mm^3 grid with attenuation correction and 1000 iterations. CT scan was performed using NanoPET/CT *In Vivo* Preclinical Imager (Mediso, Hungary) with X-ray voltage of 45 kVp, exposure time of 1100 ms and a pitch of 1. A total projection of 240 projects over 360° of rfotation was acquired. Projection data were rebinned by 1:4 and reconstructed using Butterworth filter. Image files of FLECT and CT scan were then coregistered, fused, analyzed and quantified using the analysis software InVivoScope version 2.00.

IVIS® Lumina

Anesthetized animals or their dissected organs were placed in an IVIS® Lumina Series II Imaging System (Caliper Life Sciences, USA). Fluorescence images were obtained by a charge-coupled device (CCD) camera using the XFO-12 fluorescence equipment with appropriate filter combination (excitation filter 710–760 nm, emission filter 810–875 nm) and automated exposure time. Reflected light photographic pictures were also taken during illumination. Both fluorescence and photographic images were overlayed, processed and analyzed using Living Image 4.4 software.

Histological analysis

Tissue sections of 6 µm were prepared from formalin fixed carotid arteries or lungs. For CD41-immunohistochemical 3,3'-Diaminobenzidine (DAB) staining, tissue sections were blocked with normal serum, avidin and biotin (Vector Laboratories, USA) solutions before exposure to rat anti-mouse CD41 IgG antibody (AbD Serotec, clone: MWReg30) or isotype Ig control at 5 µg/mL for overnight incubation at 4 °C. Subsequent steps were performed using Vectastain ABC kit (Vector Laboratories) in which sections were incubated with biotinylated anti-rat IgG antibody and followed by ABC reagent. The stain was developed using 3,3'-Diaminobenzidine (*DAB*)-peroxidase substrate for 5 minutes. The sections were counterstained with Mayer's Hematoxylin and slides mounted. The section was examined under the microscope for brown DAB stains which indicates presence of platelet-specific CD41. For Fluorescence Microscopy, tissue sections were blocked with 5 % bovine serum albumin (BSA) in PBS before exposure to rat anti-mouse CD41 IgG antibody (AbD Serotec, clone: MWReg30) or isotype Ig control that is directly conjugated with Allophycocyanin (APC) dye at 5 µg/mL for overnight incubation at 4 °C. Sections were washed 3 times in PBS and then imaged using Nikon BX61 Fluorescence Microscope.

Statistical Analysis

All quantitative data are reported as mean ± one standard deviation. Statistical analysis was performed using (GraphPad Prism Software Version 6). Mann-Whitney nonparametric statistical test was used for Figures 3C, 6B and S4-FLECT *in vivo* Signal. Two-way ANOVA followed by Sidak's multiple comparisons test for multiple-group analysis was used for Figures 4E-Biodistribuition, S2 and S4-IVIS *ex vivo* signal. Pearson's correlation test was used for correlation analysis for Figures 3E and 4D-radiance vs thrombus weight. Test results were considered statistically significant at values $p < 0.05$.

Results

Production of NIR-scFv fluoroprobe (Targ-Cy7) using a two-step conjugation system

A two-step conjugation system involving a sortase enzymatic reaction and a copper-free azide-cycloaddition click-chemistry reaction was used to produce the novel recombinant fluoroprobe and control (Figure 1). In the first step, targeting-scFv ($scFv_{Targ}$) with the sortase amino-acid tag of LPETGG ($scFv_{Targ}$-LPETGG; ~37kDa) was cloned and purified as previously described [19]. Using the Sortase A enzymatic reaction, the tag allowed the incorporation of a cyclooctyne compound, bicyclo-[6.1.0]-non-4-yne (BCN), carrying a glycine residue on the N-terminus. This enzymatic reaction also resulted in the removal of His-tag on the scFv, forming the end-product of BCN-Targ (Figure 1A). BCN-Targ was then conjugated to an azide-NIR dye (azide-Cyanine 7 dye) via the copper-free click reaction to generate the FLECT fluoroprobe. Free dye was removed by centrifugal filtration (MWCO:10 kDa) before overnight dialysis against PBS. The purified fluoroprobe (Targ-Cy7) was analyzed on a protein gel, and NIR signal of Cy7 from the band of interest (~33kDa) was confirmed using the Odyssey Imager, 800 nm (Figure 1B).

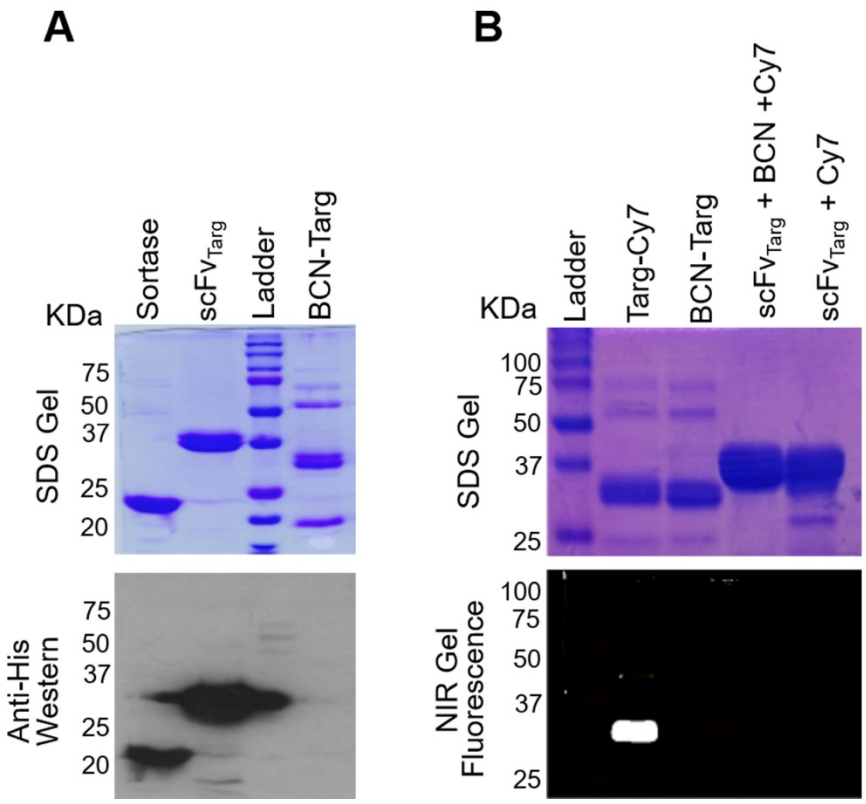

Figure 1: Two-step conjugation of scFv$_{Targ}$ for the production of FLECT fluoroprobe. A) Sortase bioconjugation of the targeting-scFv (scFv$_{Targ}$) to BCN resulted in the enzymatic product, BCN-Targ, of smaller protein size on the SDS PAGE gel (37 versus 33 kDa) due to cleavage of the His$_6$-tag (Anti-His Western). B) The BCN-scFv was then conjugated to Cy7 dye via copper-free azide-cycloaddition 'click' reaction, generating the FLECT fluoroprobe (Targ-Cy7). Protein-gel analysis of the fluoroprobe was demonstrated to have NIR fluorescence (Odyssey Scan) on the band of interest (33 kDa), not seen on its unclicked-dye control (BCN-Targ) or addition of Cy7-dye to scFv$_{Targ}$ with or without exogenous BCN (non sortase-conjugated).

In vitro functional analysis of the fluoroprobe

As a control NIR-fluoroprobe (Mut-Cy7), mutated version of the non-binding scFv (scFv$_{Mut}$), was similarly generated using the two-step system above. Both Targ-Cy7 and Mut-Cy7 were analysed on a protein gel, and under the Odyssey Imager Cy7-NIR fluorescence was detected on both bands of interest (~33 kDa) at the 800 nm channel (Figure 2A). These fluoroprobes were prepared, quantified and stored at -20°C. Functional *in vitro* analysis of the FLECT fluoroprobe was performed prior to its *in vivo* use. First, platelet-rich thrombi were formed from plasma collected from healthy volunteers by the addition of thromborel, a tissue factor that causes platelet activation. These thrombi were then incubated with either targeted fluoroprobe or its control at 2 µg/mL before they were washed to remove unbound fluoroprobe. Thrombus incubated with Targ-Cy7, and not Mut-Cy7, showed 800 nm Cy7-NIR signal as the targeted fluoroprobe bound onto the activated-platelets (Figure 2B left-panel top). Next, resting mouse platelets were isolated *ex vivo* and stimulated by platelet agonist, adenosine diphosphate (ADP), in the presence of Targ-Cy7 or Mut-Cy7 fluoroprobe. Here, only platelets activated in the presence of targeting fluoroprobe resulted in the expected NIR fluorescence, as compared to mutated fluoroprobe or non-activated platelet controls (Figure 2B left-panel bottom). Similarly, a specific fluorescence signal were only detected on transfected CHO cells expressing the activated GPIIb/IIIa platelet-receptor and not on cells expressing the resting form of this receptor or the non-transfected wild-type cells (Figure 2B right). The newly generated NIR fluoroprobe retained its specificity and affinity to activated-platelets.

As Cy7-fluorescence cannot be detected by available microscopes and existing flow cytometers, we have generated a version of the fluoroprobe and its control with the Cy5 dye for these assays using the same described two-step conjugation system (Targ-Cy5 and Mut-Cy5). Specific targeting of this probe to activated platelets but not resting platelets is demonstrated using flow cytometry (Figure S1A) and fluorescence microscopy (Figure S1B). Using stably transfected CHO cells, the binding of this probe (Targ-Cy5) is also limited to CHO cells expressing the activated form of GPIIb/IIIa (Figure S3). See Supplementary material.

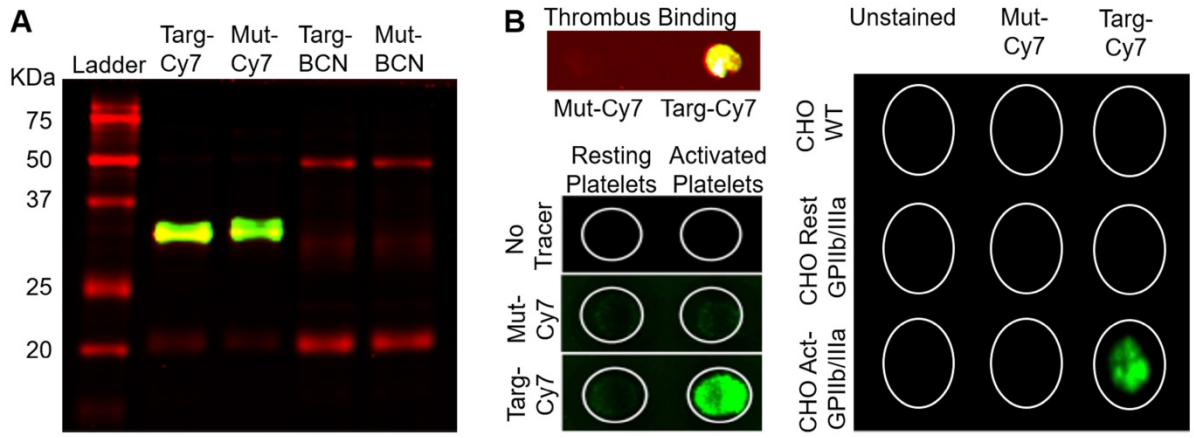

Figure 2: Binding specificity of targeting-fluoroprobe (Targ-Cy7) to activated-platelets. A) Both targeting- (Targ-Cy7) and mutated- (Mut-Cy7) fluoroprobes were produced using the two-step conjugation system as evidenced by NIR fluorescence on the bands of interest (33 kDa), while controls Targ-BCN and Mut-BCN lacked any Cy7-800 nm fluorescence. B) The functionality of the Targ-Cy7 after the conjugation to bind activated-platelets was also ascertained. Ability to bind activated-platelet-rich thrombus (Figure 2B top left panel: yellow indicating Cy7-800 nm fluorescence), *in vitro* activated-platelets (Figure 2B bottom left panel: green indicating Cy7-800 nm fluorescence) and CHO cells expressing the activated GPIIb/IIIa (Figure 2B right panel: green indicating Cy7-800 nm fluorescence) was only limited to the targeting FLECT fluoroprobe, Targ-Cy7.

Circulatory half-life of the FLECT fluoroprobe and its use in FLECT/CT of mice with ferric chloride-induced carotid thrombosis

The time taken for the blood clearance of Targ-Cy7 was next determined prior to its use as an imaging fluoroprobe. Mice were intravenously given Targ-Cy7, and NIR-signal that related to its circulation in the blood was ascertained using the IVIS® Lumina scanner (excitation filter 710–760 nm, emission filter 810–875 nm) and shown in Figure 3A. The detected NIR signal peaked at 5 min post injection and this level dropped by half in about 96.8 min. After verification of its *in vitro* functionality and blood clearance, the fluoroprobe was then used for *in vivo* FLECT detection of mouse thrombosis. Mouse left carotid vessel was exposed to ferric chloride to induce thrombosis. Mice were then injected with either Targ-Cy or Mut-Cy7 fluoroprobe and allowed to circulate for 45 min before they were scanned in the FLECT imager to detect 3-dimensional NIR fluorescence within the body. This was immediately followed by computed tomography (CT) imaging to determine the anatomical structure of the mouse and thereby provide a detailed location of any detected fluorescence signals. After reconstruction and image analysis, the thrombus was clearly detected in animals injected with the Targ-Cy7 fluoroprobe and not the control fluoroprobe (Figure 3B). This signal was localized to the left side of the mouse and not on the healthy right carotid vessel. Quantification of fluorescence intensity in the regions of interest, where the thrombus was located, clearly showed Targ-Cy7 fluoroprobe resulted in remarkably higher levels of detected signals as compared to low background levels in mice with Mut-Cy7 fluoroprobe (Figure 3C, n=6 per group, p= 0.0022). This demonstrated the ability of the FLECT imager to detect *in vivo* thrombus using the specific fluoroprobe. Histological analysis of the carotid vessels was later performed to confirm the presence of platelet-rich thrombus on the left vessel of all mice (Targ-Cy7 and Mut-Cy7) in this study while the right vessel remained healthy (Figure 3D). Detailed analysis of the detected Targ-Cy7 FLECT signal in each left-carotid artery showed a strongly significant correlation to its thrombus weight (Figure 3E; p= 0.0006 and r= 0.9807 using the Pearson's correlation test).

IVIS® imaging for *ex vivo* verification and quantification of the FLECT signal

To confirm and further quantify the detected FLECT signal, IVIS® Lumina 2-dimensional scanner was used with the ability to excite and detect Cy7 probe, as seen in Figure 3A. Upon completion of FLECT/CT scans, mouse was placed in the Lumina scanner in a supine position with the injury site exposed to the laser and detector (Figure 4, n=6). The Lumina image clearly detected Targ-Cy7 fluoroprobe, and not Mut-Cy7, at the site of thrombus formation (Figure 4A, top). After euthanasia and perfusion, both injured left and healthy right carotid vessels of the animal were collected and similarly scanned in the Lumina. This *ex vivo* scanning detected Cy7 fluorescence in only the injured left vessel (Figure 4A, bottom) injected with Targ-Cy7. These data ascertain that the targeting NIR fluoroprobe unequivocally binds onto the thrombus in the mouse, resulting in their optical fluorescence detection. To perform fluorescence biodistribution of this fluoroprobe, different major organs of the mouse were also

collected and scanned in the Lumina imager (Figure 4B). The detected fluorescence in each organ was quantified (Figure 4C, non-normalized radiance values to respective organ weights) and only in the injured vessel of mice injected with Targ-Cy7 significant fluoroprobe uptake was noted, as compared to non-targeting control (Figure 4E; Radiance/mg of organ; n=6; Left Carotid (injured) p= 0.0012; all other organs p > 0.9999). Thus using the Lumina scanner, the NIR signal detected by the FLECT/CT imager was verified, quantified and localized to the injured vessel. Further analysis of the detected *ex vivo* Targ-Cy7 IVIS signal in each left-carotid artery showed a significant correlation to its thrombus weight (Figure 4D; p= 0.0303 and r= 0.8544 using the Pearson's correlation test).

In addition to the described non-occlusive thrombosis model, Targ-Cy7 FLECT imaging was successfully employed to detect fully occluding thrombi (see supplementary Figure S4). However, in the complete occlusive model the detected *in vivo* FLECT and ex vivo IVIS signals were both lower than those observed in the non-occluded thrombus. Besides, no significant correlation was observed between the detected signals and the respective thrombus weight (data not shown). Taken together, these data suggest that there was less binding of the Targ-Cy7 to the fully occluded thrombus probably due to the limitation in blood circulation carrying the fluoroprobe evenly to all the thrombus areas.

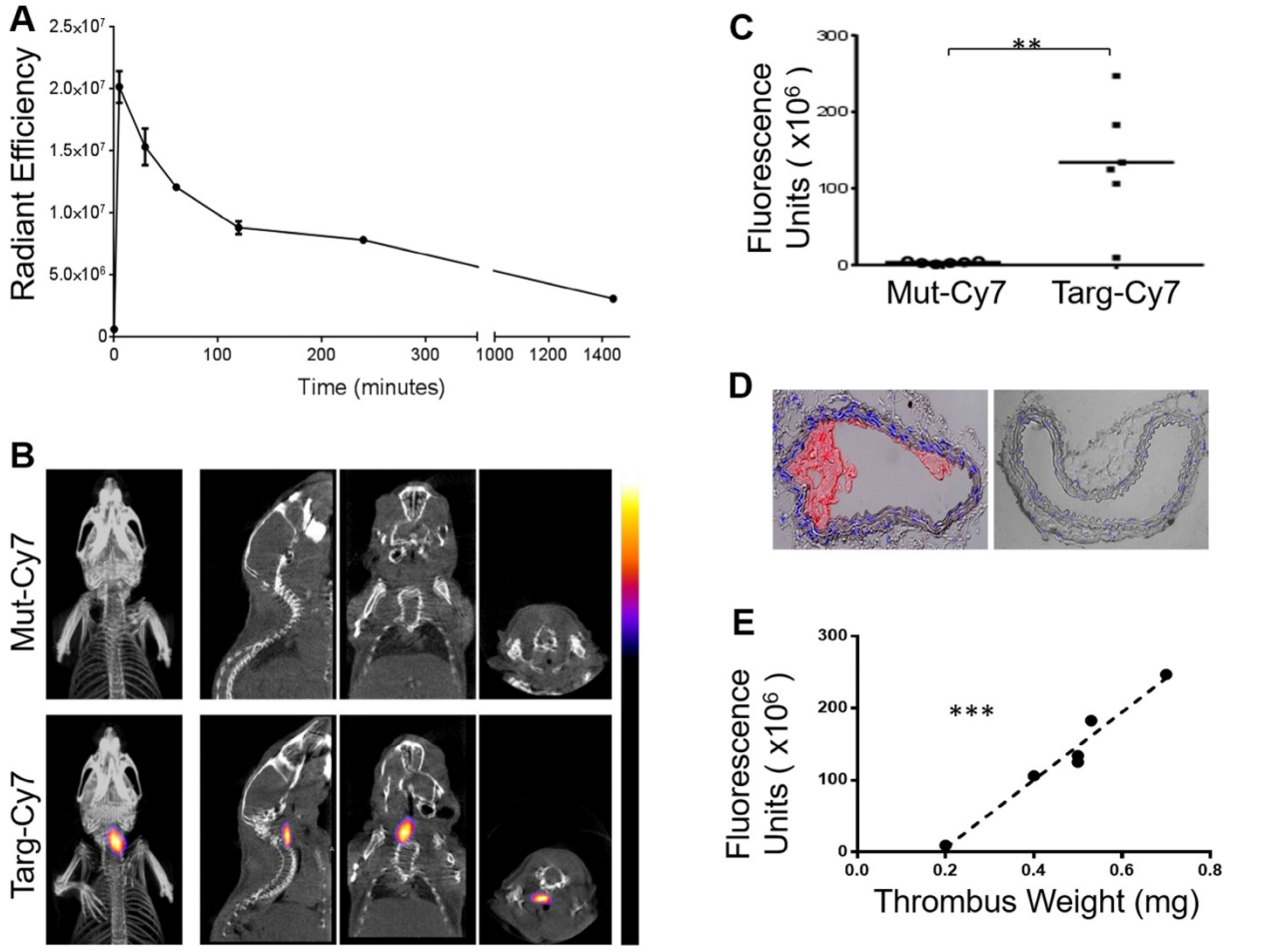

Figure 3: Circulatory *in vivo* half-life of the FLECT fluoroprobe and its use in FLECT/CT imaging of mice with left carotid ferric chloride induced thrombus. A) Mice (n=5) were i.v. injected with 1 µg/g of Targ-Cy7 and blood was collected at different time-points (0, 5, 30, 60 120, 240 and 1440 minutes). The NIR fluorescence signal in the collected samples was determined by the IVIS® Lumina imager and quantified as shown. B) Upon arterial thrombus formation using the ferric chloride model, mice were i.v. injected with either mutated (Mut-Cy7; top panel) or targeting-fluoroprobe (Targ-Cy7; bottom panel) and allowed to circulate before they were scanned on the FLECT/CT imager. Following data reconstruction, coregistration and analysis, a representative comparison of maximum-intensity projection of FLECT/CT images of Mut-Cy7 (n=6) and Targ-Cy7 (n=6) mice is shown. The colour scale for each FLECT/CT image shows levels of detected NIR fluorescence with white corresponding to the highest intensity and blue the lowest. C) Using Invivoscope software, the region of interest around the left carotid artery was determined, and detected fluorescence intensity was quantified between groups of mice (**: p ≤ 0.01; Mann-Whitney nonparametric test, p= 0.0022). D) A representative micrograph of the ferric chloride-injured carotid artery (top) and the contralateral uninjured carotid artery (bottom), where nuclear stain (DAPI) is blue, and platelet-specific (CD41- Allophycocyanin) is red. E) Further analysis of the detected FLECT-signal in each mouse shows a strongly significant correlation to the weight of its *ex-vivo* thrombus (using Pearson's correlation analysis: r = 0.9807 and p= 0.0006, ***).

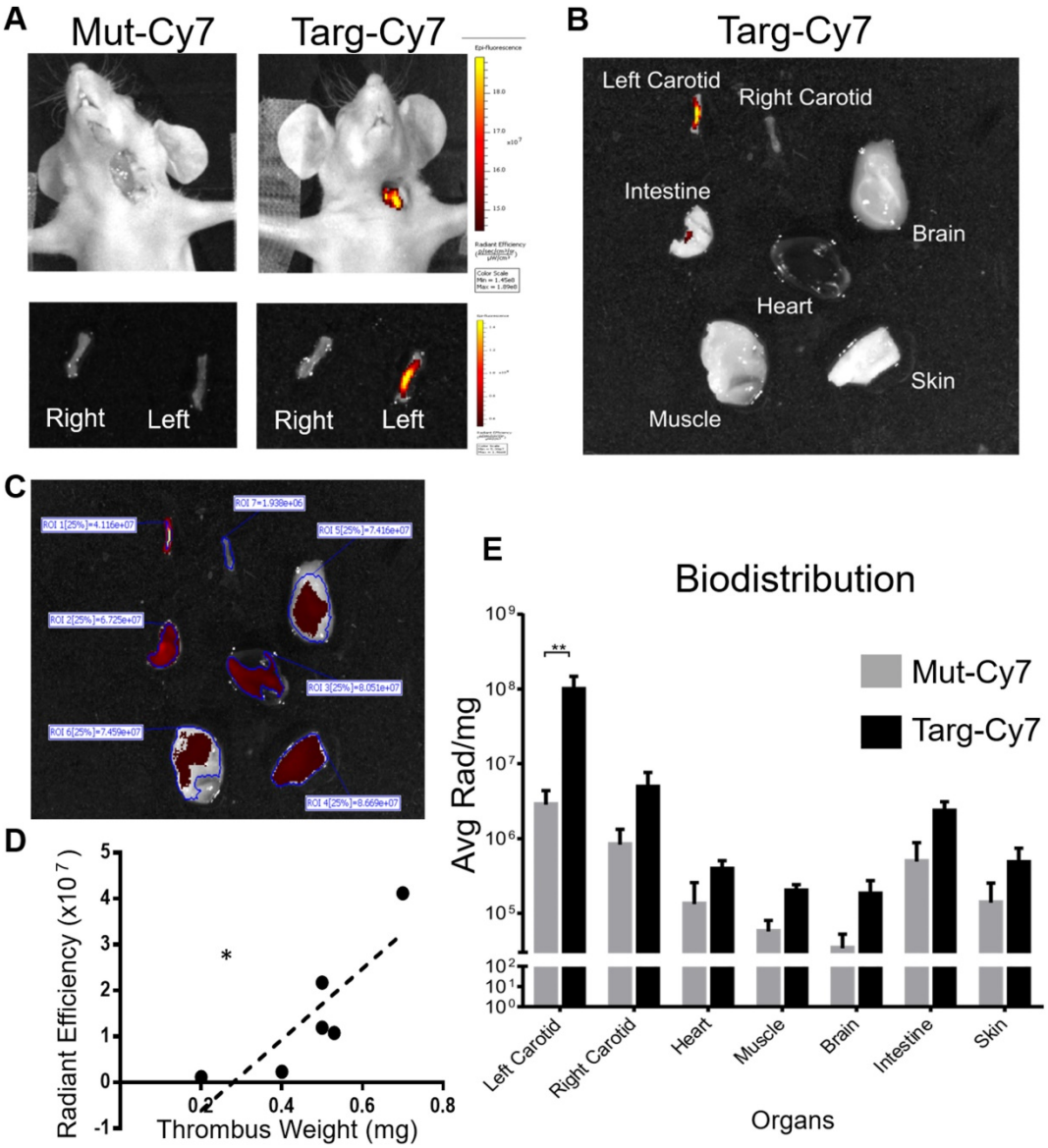

Figure 4: IVIS® Lumina scan of mice and their organs post FLECT/CT imaging. A) To verify the detected FLECT signal, each animal was subsequently imaged in the two-dimensional planar IVIS® Lumina scanner. After euthanasia, both the right (uninjured) and left (injured) carotid arteries of each mouse were collected and similarly scanned in the IVIS® Lumina scanner (Figure 4A, bottom panel). B) In addition, major organs were also collected and scanned *ex vivo*. C) Quantitative analysis of the scanned organs with a region of interest (ROI) set at a fluorescence threshold of 25% was used to determine the levels of detected light radiance (un-normalized radiance to organ weight is shown). D) Analysis of the levels of detected *ex vivo* Targ-Cy7 signals of each injured left carotid vessel shows a significant correlation to its thrombus weight (using Pearson's correlation analysis (r = 0.8544 and p = 0.0303, *). E) Biodistribution of the NIR fluoroprobe uptake of these organs was also calculated by dividing the radiance with the mass (mg) of each scanned tissue for each group of mice (n=6) (Figure 4E; Two-way ANOVA-Sidak's multiple group comparison test between Targ-Cy7 and Mut-Cy7 groups, Left Carotid- p= 0.0012. The p values between the 2 groups for rest of the organs (Right Carotid, Heart, Muscle, Brain, Intestine and Skin) are all >0.9999).

FLECT/CT imaging to monitor therapeutic efficacy

To demonstrate the ability of the FLECT/CT scanner to be used as a monitoring tool of treatment efficacy, ferric chloride injured mice were injected with Targ-Cy7 and scanned before and after a combined thrombolytic and anti-platelet treatment with urokinase/integrilin drugs (Figure 5). As expected, accumulation of the Targ-Cy7 fluoroprobe in the thrombus of the left carotid vessel was detected in mice before treatment by the FLECT/CT imager (n=3). After this initial scan, mice were treated with either urokinase/integrilin therapy to disrupt the formed thrombus or PBS as control before they were imaged again on the FLECT/CT scanner. Post-urokinase/integrilin-treatment scan, and not PBS-treated mice, revealed the disappearance of the previously detected Cy7-NIR signal in the thrombus area, suggesting the success of such thrombus-resolving therapy. This was later confirmed using *ex vivo* Lumina imaging of the injured vessel of both treatment groups and histological analysis that

revealed the loss of NIR signal and thrombus following urokinase/integrilin therapy (Figure 5B). Histological analysis similar to Figure 3D was also performed (data not shown).

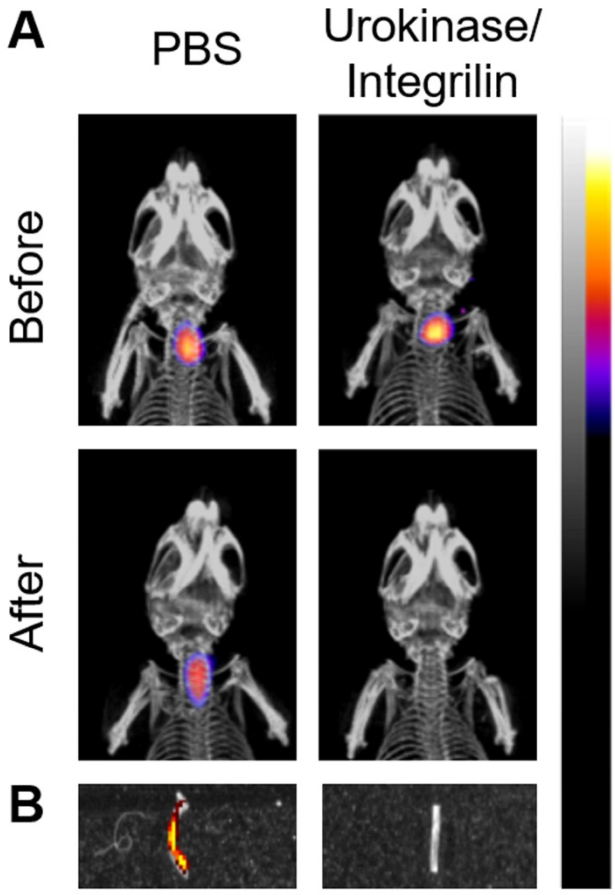

Figure 5: Monitoring of antithrombotic therapy in mice using FLECT/CT. Thrombus was induced in the left carotid artery of mice by ferric chloride before the i.v. injection of activated-platelet targeting fluoroprobe, Targ-Cy7. A) Representative comparison of maximum-intensity projection FLECT/CT images of mice before and after treatment with either PBS or combined thrombolytic/anti-platelet drugs, urokinase/integrilin (n=3). The colour scale for each FLECT/CT image shows levels of detected NIR fluorescence, with white corresponding to the highest intensity and blue the lowest. B) The injured carotid artery was collected from each treated animal and scanned on the IVIS® Lumina imager to confirm the detected FLECT NIR signal. A representative image of both control (PBS-treated) and urokinase/integrilin-treated left carotid vessels is shown. Detected Lumina fluorescence signal is depicted accordingly.

Pulmonary embolism FLECT/CT diagnosis

After the success of FLECT/CT to diagnose ferric chloride model of artery thrombosis, we next determined if FLECT/CT imaging can detect pulmonary embolism caused by venous thrombosis, which is a frequent cause of death and is difficult to diagnose clinically. There is clearly the need for better non-invasive imaging technologies. Mice were injected intravenously with thromborel to induce platelets activation and formation of thrombus that lodged in the lungs microvasculature, resulting in pulmonary embolism. Fluoroprobes were injected and allowed to circulate for 45 minutes upon observation of breathing difficulties in mice following thromborel injection. Mice were then scanned on the FLECT/CT imager and pulmonary embolism was diagnosed in mice with Targ-Cy7 fluoroprobe (n=4) and not in mice with the control-fluoroprobe (n=3) (Figure 6A). As the lungs were not contrasting to be imaged on the CT scan, contrast agent was perfused into the organ after euthanasia and mice were rescanned to ensure that detected FLECT signal indeed localized in the lung (Fig 6A, bottom panel). Quantification of the region of interest showed significantly higher levels of fluorescence signal of Targ-Cy7 mice than its control-fluoroprobe ($p = 0.0286$) (Figure 6B). Further *ex vivo* and histological analysis of the lungs confirmed the signals were related to the CD41-positive thrombus in the lungs (Figure 6C).

Discussion

Here we demonstrated the use of a novel three-dimensional, fluorescence-based imaging modality, FLuorescence Emission Computed Tomography (FLECT), in the context of thromboembolic diseases. Results from both the ferric chloride injury and thromborel-induced pulmonary embolism models have shown that FLECT imaging, in combination with a scFv-based NIR probe that targets activated-platelets, could sensitively detect and accurately localize the site of thrombosis in both arterial and venous circulations. Further, serial studies to monitor response to treatment (e.g. resolution of thrombus when treated with urokinase/integrilin) were demonstrated to be feasible. While not directly tested in our study, we believe this imaging modality would also be useful in the surveillance of disease progression with an appropriate biomarker-based fluoroprobe. In addition to the FLECT scan, we have also demonstrated the flexibility of our NIR-fluoroprobe for use in *in vitro* assays (thrombus-binding and activated-platelet binding using the Odyssey scanner), *ex vivo* organ imaging (IVIS® Lumina) and *in vivo* IVIS® Lumina scanning. To our knowledge, this is the first report to describe the use of a novel recombinant NIR fluoroprobe on the FLECT imaging platform. Importantly, we believe these findings may have significant implications in preclinical animal research, clinical diagnosis and therapy.

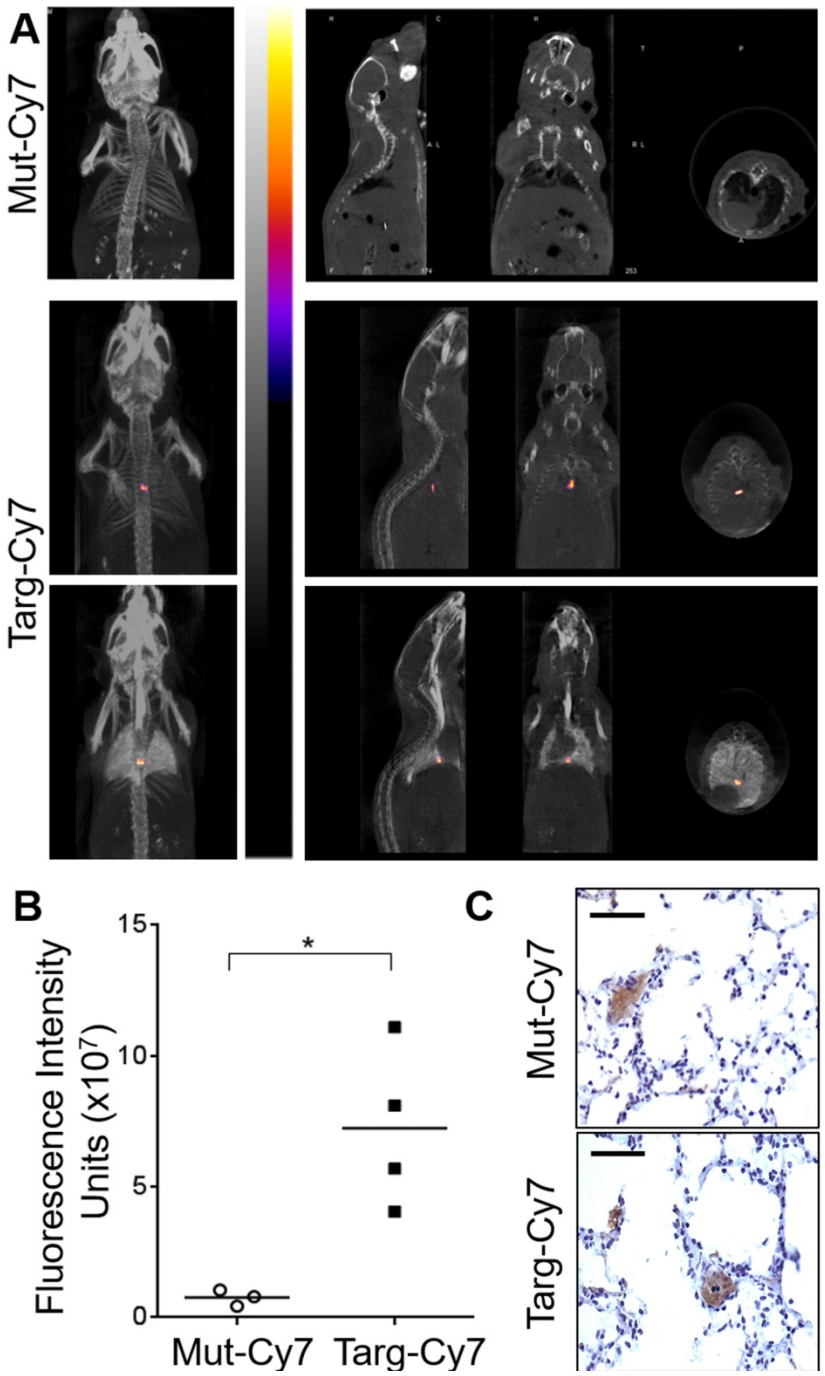

Figure 6: FLECT/CT imaging of mice with pulmonary embolism. Pulmonary embolism was induced in mice by the injection of thromborel. A) Following induction of embolism, mice were given (i.v.) either non-targeting (Mut-Cy7, n=3) or activated-platelet targeting-fluoroprobe (Targ-Cy7, n=4). Mice were then imaged in the FLECT/CT imager and generated images were reconstructed and analyzed as shown. To ensure the detected NIR signal in the Targ-Cy7 animal was localized to the lungs, mice were subsequently euthanized and airway perfused with CT contrasting medium, Iopromide, before an additional scan was performed (bottom panel). B) NIR fluorescence intensity from the region of interest was quantified in both groups (Mann-Whitney nonparametric test, p= 0.0286). C) Lungs were collected and histological analysis performed to detect CD41 positive (DAB stain; brown) thrombi within the pulmonary vessels. Each scale bar represents 20 μm of the micrograph.

In preclinical settings, recent advances in molecular imaging have helped to elucidate some of the underlying pathological processes along with the complex interplay between different cells and molecules of several diseases. Moreover, molecular imaging has been proven to be invaluable in the non-invasive assessment of disease progression and therapeutic efficacy. This has been largely driven by advances in sophisticated *in vivo* imaging modalities and the development of highly-specific imaging probes. Over recent years, great strides have been made in *in vivo* whole-animal imaging using various imaging modalities including magnetic resonance (MRI), positron emission tomography (PET) and

FLECT. Of which, FLECT is of particular interest, as it has unique advantages over PET and MRI.

For FLECT imaging, a fluorescence probe is used. It requires photon excitation of the probe resulting in the emission of optical signals, which can be detected by the FLECT imager. In the past, the use of such an optical modality was limited by poor signal-noise ratios, impaired signal penetration as a result of the absorbance of excitation photons by surrounding off-target tissues and excessive noise due to tissue autofluorescence. However, identification of the "optical window" of NIR photoactivity between 700 nm to 1000 nm has revolutionized the field, where it was found that within this spectrum, tissue absorbance, light scattering and autofluorescence are low and thus significantly improve "signal-to-background" (SBR) ratio [25-27]. Consequently, there has been great enthusiasm to develop various NIR probes that emit within these wavelengths, including cyanine dyes, squaraine derivatives, porphyrin derivatives and borondipyrromethane analogs and IRDyes. Cyanine dyes such as Cy5.5, ICG and Cy7, are excellent NIR probes, possessing high molar absorptivity, good photostability and strong fluorescence emission. Of these, Cy7, as used in this study, has been shown to be the superior dye of the cyanine dyes [28]. Other newer imaging probes such as the zwitterionic (ZW) 800 NIR fluorophore promises even better SBR with a rapid circulation and organ clearance [29].

Besides generating new NIR probes, novel designs are being introduced to existing probes to limit their fluorescence emission only upon binding to targets of interest and thus ensuring a clear background. For example, fluorophore-quencher probes (Cy7 probe-SiNQ dark quencher) based on the Forster resonance energy transfer (FRET) mechanism has been shown to greatly reduce *in vivo* background signals with enhanced specificity due to fluorescence emission only being detected upon 'probe activation' in bio-environments of interest [30-32]. Taking all these together, we can expect the generation of many more advanced FLECT-probes in the near future which will deliver significantly better FLECT-image quality.

As mentioned above, compared to other imaging modalities, FLECT has unique advantages. PET is a nuclear imaging modality that involves the use of positron-emitting radionuclide which emits gamma rays for detection. However, the use of ionising radiation has safety implications for both researchers and animals. Further to this, the properties of radionuclides also pose significant challenges in the design and planning of experiments; decay in radioactivity restricts the run time of an experiment, and necessitates compensation to account for the differences in detected radioactivity between scans and the biodistribution of gamma counter measurements. In addition, radionuclide production is highly regulated and supplied on a fixed schedule for scanning, and thus requires meticulous planning for both basic science and clinical use. In contrast, fluorescent probes can be synthesized in large-quantities, quality-assessed and stored for later-use. This permits fluoroprobe standardisation between different scanning days and, importantly, avoids the use of ionising radiation, a significant advantage of the technique.

MRI is another imaging modality used clinically, with the advantage of not using ionising radiation. However, compared to MRI, FLECT scanning has the potential to detect multiple targets in one study by the use different targeting-fluoroprobes with unique excitation and emission spectra. This provides the opportunity to determine the specific roles of various proteins, cells and/or drugs of interest during a biological process (e.g. a drug interaction with cancer cells) and ascertain a deeper *in vivo* understanding of specific interactions in one setting. Thus, much more information can be obtained from a single experiment.

In our study, we use a scFv, specific for activated GPIIb/IIIa on platelets, to detect thrombosis. This approach has the advantage of detecting a particular biological process of interest. In addition, this approach is versatile. We have previously conjugated scFv with probes used in other imaging modalities and showed that thrombosis can be detected via targeted MRI [15, 16], ultrasound [14, 23] and PET [12] imaging. This advantage is of particular relevance in clinical settings, as these imaging facilities are available in more and more hospitals. The success of our current study using activated-GPIIb/IIIa-scFv has set the foundation for future work examining the utility of other scFvs/peptides-based fluoroprobes (e.g. Fab fragment and designed ankyrin repeat proteins) targeting different molecular markers of coagulation and inflammation, which can be used to generate an array of specific fluoroprobes for FLECT imaging of various cardiovascular and inflammatory diseases. By targeting different components of inflammation and coagulation, we can better delineate and understand the molecular processes of these pathologies. It is also expected that the sensitive of FLECT imaging will improve with the use of better molecular targets for the disease. For example, given pulmonary embolus is usually fibrin-rich, fibrin-specific antibody would theoretically provide stronger and more specific signals. Whilst antibody against human fibrin had been developed [33], antibody targeting mouse fibrin is not currently

available for us to test this hypothesis

Besides thrombosis, activated-platelets have recently been recognized to be involved in many inflammatory processes [6, 7] including atherosclerotic plaque rupture [17, 34], ischemia/reperfusion injury [35-37], multiple sclerosis [38-40] and rheumatoid arthritis [41-44]. In some of these settings, however, the role of platelets is not well defined. As our approach provides a way to detect, localize and track platelets *in vivo*, this could allow for further investigation into the role of platelets in these inflammatory diseases.

Our result is also of significant clinical importance. We believe that this technology has the potential to improve radiological diagnostic accuracy of arterial thrombosis; especially stroke is a good example of this. Currently, timely diagnosis of stroke relies on non-contrast CT and CT angiography (CTA), which are relatively insensitive at detecting ischemic changes and culprit thrombi at the acute phase of stroke [45, 46]. Envisaging that CT scanners may in the future include FLECT imaging capabilities, such as those currently used in small animal research today, FLECT imaging has the potential to enhance diagnostic sensitivity allowing early diagnosis and thereby rapid treatment of stroke victim. In addition, FLECT imaging may also find a role in the detection of intracardiac thrombi and may serve as a non-invasive alternative to transesophageal echocardiography in the clinical setting of excluding left atrial thrombi before electric defibrillation in patients presenting with atrial fibrillation. In terms of venous thrombosis, FLECT may be particularly useful, as it spares uses of ionizing radiation. For example, pregnancy is a major risk factor of pulmonary embolism [47]. Medical imaging currently used to diagnose pulmonary embolism involves ionising radiation, with inherent teratogenic and carcinogenic risks, and therefore ideally should not be used on pregnant women. Thus, clinical translation of our study could fill a major unmet medical need and be a useful tool to monitor platelet-mediated diseases during pregnancy.

Indeed, investigators have started to translate FLECT use from preclinical to clinical settings and fluorescence-based probes and detection equipment have been developed for superficial and optically accessible organs including human eyes and joints (ICG; FDA approved [48]). For example, infrared-reflectance based retinal scanning (Heidelberg Engineering) is available for clinical use, and should have the capacity to detect the fluoroprobe described in this report. This could be useful in the detection of optic neuritis, a condition highly prevalent amongst patients with multiple sclerosis. Similarly, in combination with a NIR scanner (Xiralite, Mivenion, GmbH), a non-specific ICG fluoroprobe has been used to detect joint hypervascularization in patients with rheumatoid arthritis [49]. FLECT Imaging of deep-seated organs or pathology (e.g., arterial and venous thrombosis) in clinical settings remains a challenge. However, with anticipated advances in optical technologies and computer algorithms, such hurdles may be overcome in the near future. For example, changing the orientation of scanner setups (e.g. using trans-illumination instead of epi-illumination) has much improved the ability to detect deeply seated fluorophores. Further, integrating CT and FLECT into one scanner has refined its spatial resolution and allows precise anatomical localisation of the fluorescence signals. Better signal to noise ratio and elimination of autofluorescence can also be achieved with sophisticated spectral processing such as liquid crystal tunable filters [27]. A clinical area in which the promises of FLECT technology with its current tissue penetration are already discussed is the imaging of joints in diseases such as rheumatoid arthritis [50]. As platelets and platelet-derived microparticles are known to be involved in early rheumatoid arthritis [41], our newly designed NIR fluoroprobe may be well suited to detect this disease in its early development."

In summary, we have demonstrated that using a unique immuno-NIR probe, we can non-invasively detect and monitor thromboembolism *in vivo* in whole-animals by FLECT imaging. This is an invaluable tool for preclinical research, both in understanding the mechanisms of thrombosis and embolism, and the developmental testing of new antithrombotic drugs. Overall, with its non-radiation nature, low-cost and high sensitivity, this rapidly developing scanning technology for the fluorescence imaging of thrombosis and embolism could play an increasing role in clinical settings.

Supplementary Material

Supplementary figures.
http://www.thno.org/v07p1047s1.pdf

Acknowledgements

The authors would like to thank Mr Cameron Nowell for his technical support in the running of the FLECT, CT and IVIS scanners. This work is funded by the National Health and Medical Research Council (NHMRC). K.P is a NHMRC Principal Research Fellow. M.L.Y is supported by an Australian Postgraduate Award (APA) scholarship. A.L.H. is supported by the National Heart Foundation Postgraduate scholarship. X.W. is National Heart Foundation Postdoctoral Fellow.

Authorship Contributions

B.L. and K.P. designed the study. B.L., Y.Y., M.L.Y., A.L.H., U.F., J.P., M.Z. and X.W. performed experiments and collected the data. B.L., Y.Y., M.L.Y., A.L.H., U.F., J.P., M.Z. and K.P. analyzed the data. B.L., Y.Y., A.L.H. and K.P. wrote the manuscript.

Conflict of Interest

K.P. is inventor on patents describing activated platelet-targeting recombinant antibodies. All other authors have declared that no conflict of interest exists.

References

1. Ntziachristos V. Going deeper than microscopy: the optical imaging frontier in biology. Nat Methods. 2010; 7: 603-14.
2. Ntziachristos V. Fluorescence molecular imaging. Annu Rev Biomed Eng. 2006; 8: 1-33.
3. Escobedo JO, Rusin O, Lim S, Strongin RM. NIR dyes for bioimaging applications. Curr Opin Chem Biol. 2010; 14: 64-70.
4. Umezawa K, Citterio D, Suzuki K. New trends in near-infrared fluorophores for bioimaging. Anal Sci. 2014; 30: 327-49.
5. Hansson GK. Inflammation, atherosclerosis, and coronary artery disease. N Engl J Med. 2005; 352: 1685-95.
6. Rondina MT, Weyrich AS, Zimmerman GA. Platelets as cellular effectors of inflammation in vascular diseases. Circ Res. 2013; 112: 1506-19.
7. Ioannou A, Kannan L, Tsokos GC. Platelets, complement and tissue inflammation. Autoimmunity. 2013; 46: 1-5.
8. Gawaz M, Langer H, May AE. Platelets in inflammation and atherogenesis. J Clin Invest. 2005; 115: 3378-84.
9. Lievens D, von Hundelshausen P. Platelets in atherosclerosis. Thromb Haemost. 2011; 106: 827-38.
10. Fuentes QE, Fuentes QF, Andres V, Pello OM, Font de Mora J, Palomo GI. Role of platelets as mediators that link inflammation and thrombosis in atherosclerosis. Platelets. 2013; 24: 255-62.
11. Go AS, Mozaffarian D, Roger VL, Benjamin EJ, Berry JD, Blaha MJ, et al. Heart Disease and Stroke Statistics—2014 Update. Circulation. 2013; 129: e28-e292.
12. Ardipradja K, Yeoh SD, Alt K, O'Keefe G, Rigopoulos A, Howells DW, et al. Detection of activated platelets in a mouse model of carotid artery thrombosis with 18 F-labeled single-chain antibodies. Nucl Med Biol. 2014; 41: 229-37.
13. Hohmann JD, Wang X, Krajewski S, Selan C, Haller CA, Straub A, et al. Delayed targeting of CD39 to activated platelet GPIIb/IIIa via a single-chain antibody: breaking the link between antithrombotic potency and bleeding? Blood. 2013; 121: 3067-75.
14. Wang X, Gkanatsas Y, Palasubramaniam J, Hohmann JD, Chen YC, Lim B, et al. Thrombus-Targeted Theranostic Microbubbles: A New Technology towards Concurrent Rapid Ultrasound Diagnosis and Bleeding-free Fibrinolytic Treatment of Thrombosis. Theranostics. 2016; 6: 726-38.
15. von Zur Muhlen C, Sibson NR, Peter K, Campbell SJ, Wilainam P, Grau GE, et al. A contrast agent recognizing activated platelets reveals murine cerebral malaria pathology undetectable by conventional MRI. J Clin Invest. 2008; 118: 1198-207.
16. von zur Muhlen C, Peter K, Ali ZA, Schneider JE, McAteer MA, Neubauer S, et al. Visualization of activated platelets by targeted magnetic resonance imaging utilizing conformation-specific antibodies against glycoprotein IIb/IIIa. J Vasc Res. 2009; 46: 6-14.
17. von Elverfeldt D, von zur Muhlen C, Wiens K, Neudorfer I, Zirlik A, Meissner M, et al. In vivo detection of activated platelets allows characterizing rupture of atherosclerotic plaques with molecular magnetic resonance imaging in mice. PLoS One. 2012; 7: e45008.
18. von Elverfeldt D, Maier A, Duerschmied D, Braig M, Witsch T, Wang X, et al. Dual-contrast molecular imaging allows noninvasive characterization of myocardial ischemia/reperfusion injury after coronary vessel occlusion in mice by magnetic resonance imaging. Circulation. 2014; 130: 676-87.
19. Ta HT, Prabhu S, Leitner E, Jia F, von Elverfeldt D, Jackson KE, et al. Enzymatic single-chain antibody tagging: a universal approach to targeted molecular imaging and cell homing in cardiovascular disease. Circ Res. 2011; 109: 365-73.
20. Witte MD, Theile CS, Wu T, Guimaraes CP, Blom AE, Ploegh HL. Production of unnaturally linked chimeric proteins using a combination of sortase-catalyzed transpeptidation and click chemistry. Nat Protoc. 2013; 8: 1808-19.
21. Schwarz M, Rottgen P, Takada Y, Le Gall F, Knackmuss S, Bassler N, et al. Single-chain antibodies for the conformation-specific blockade of activated platelet integrin alphaIIbbeta3 designed by subtractive selection from naive human phage libraries. FASEB J. 2004; 18: 1704-6.
22. Stoll P, Bassler N, Hagemeyer CE, Eisenhardt SU, Chen YC, Schmidt R, et al. Targeting ligand-induced binding sites on GPIIb/IIIa via single-chain antibody allows effective anticoagulation without bleeding time prolongation. Arterioscler Thromb Vasc Biol. 2007; 27: 1206-12.
23. Wang X, Hagemeyer CE, Hohmann JD, Leitner E, Armstrong PC, Jia F, et al. Novel single-chain antibody-targeted microbubbles for molecular ultrasound imaging of thrombosis: validation of a unique noninvasive method for rapid and sensitive detection of thrombi and monitoring of success or failure of thrombolysis in mice. Circulation. 2012; 125: 3117-26.
24. Wong C, Liu Y, Yip J, Chand R, Wee JL, Oates L, et al. CEACAM1 negatively regulates platelet-collagen interactions and thrombus growth in vitro and in vivo. Blood. 2009; 113: 1818-28.
25. Frangioni JV. In vivo near-infrared fluorescence imaging. Curr Opin Chem Biol. 2003; 7: 626-34.
26. Luo S, Zhang E, Su Y, Cheng T, Shi C. A review of NIR dyes in cancer targeting and imaging. Biomaterials. 2011; 32: 7127-38.
27. Leblond F, Davis SC, Valdes PA, Pogue BW. Pre-clinical whole-body fluorescence imaging: Review of instruments, methods and applications. J Photochem Photobiol B. 2010; 98: 77-94.
28. Ballou B, Fisher GW, Deng JS, Hakala TR, Srivastava M, Farkas DL. Cyanine fluorochrome-labeled antibodies in vivo: assessment of tumor imaging using Cy3, Cy5, Cy5.5, and Cy7. Cancer Detect Prev. 1998; 22: 251-7.
29. Choi HS, Gibbs SL, Lee JH, Kim SH, Ashitate Y, Liu F, et al. Targeted zwitterionic near-infrared fluorophores for improved optical imaging. Nat Biotechnol. 2013; 31: 148-53.
30. Lee S, Cha EJ, Park K, Lee SY, Hong JK, Sun IC, et al. A near-infrared-fluorescence-quenched gold-nanoparticle imaging probe for in vivo drug screening and protease activity determination. Angew Chem Int Ed Engl. 2008; 47: 2804-7.
31. Merian J, Gravier J, Navarro F, Texier I. Fluorescent nanoprobes dedicated to in vivo imaging: from preclinical validations to clinical translation. Molecules. 2012; 17: 5564-91.
32. Myochin T, Hanaoka K, Iwaki S, Ueno T, Komatsu T, Terai T, et al. Development of a Series of Near-Infrared Dark Quenchers Based on Si-rhodamines and Their Application to Fluorescent Probes. J Am Chem Soc. 2015; 137: 4759-65.
33. Peter K, Graeber J, Kipriyanov S, Zewe-Welschof M, Runge MS, Kubler W, et al. Construction and functional evaluation of a single-chain antibody fusion protein with fibrin targeting and thrombin inhibition after activation by factor Xa. Circulation. 2000;101: 1158-64.
34. Chen YC, Bui AV, Diesch J, Manasseh R, Hausding C, Rivera J, et al. A novel mouse model of atherosclerotic plaque instability for drug testing and mechanistic/therapeutic discoveries using gene and microRNA expression profiling. Circ Res. 2013; 113: 252-65.
35. Lapchak PH, Kannan L, Ioannou A, Rani P, Karian P, Dalle Lucca JJ, et al. Platelets orchestrate remote tissue damage after mesenteric ischemia-reperfusion. Am J Physiol Gastrointest Liver Physiol. 2012; 302: G888-97.
36. Lapchak PH, Ioannou A, Kannan L, Rani P, Dalle Lucca JJ, Tsokos GC. Platelet-associated CD40/CD154 mediates remote tissue damage after mesenteric ischemia/reperfusion injury. PLoS One. 2012; 7: e32260.
37. Liu Y, Gao XM, Fang L, Jennings NL, Su Y, Q X, et al. Novel role of platelets in mediating inflammatory responses and ventricular rupture or remodeling following myocardial infarction. Arterioscler Thromb Vasc Biol. 2011; 31: 834-41.
38. Horstman LL, Jy W, Ahn YS, Zivadinov R, Maghzi AH, Etemadifar M, et al. Role of platelets in neuroinflammation: a wide-angle perspective. J Neuroinflammation. 2010; 7: 10.
39. Langer HF, Choi EY, Zhou H, Schleicher R, Chung KJ, Tang Z, et al. Platelets contribute to the pathogenesis of experimental autoimmune encephalomyelitis. Circ Res. 2012; 110: 1202-10.
40. Habets KL, Huizinga TW, Toes RE. Platelets and autoimmunity. Eur J Clin Invest. 2013; 43: 746-57.
41. Boilard E, Nigrovic PA, Larabee K, Watts GF, Coblyn JS, Weinblatt ME, et al. Platelets amplify inflammation in arthritis via collagen-dependent microparticle production. Science. 2010; 327: 580-3.
42. Boilard E, Blanco P, Nigrovic PA. Platelets: active players in the pathogenesis of arthritis and SLE. Nat Rev Rheumatol. 2012; 8: 534-42.
43. Cloutier N, Pare A, Farndale RW, Schumacher HR, Nigrovic PA, Lacroix S, et al. Platelets can enhance vascular permeability. Blood. 2012; 120: 1334-43.
44. Binstadt BA, Patel PR, Alencar H, Nigrovic PA, Lee DM, Mahmood U, et al. Particularities of the vasculature can promote the organ specificity of autoimmune attack. Nat Immunol. 2006; 7: 284-92.
45. Chalela JA, Kidwell CS, Nentwich LM, Luby M, Butman JA, Demchuk AM, et al. Magnetic resonance imaging and computed tomography in emergency assessment of patients with suspected acute stroke: a prospective comparison. Lancet. 2007; 369: 293-8.
46. Shrier DA, Tanaka H, Numaguchi Y, Konno S, Patel U, Shibata D. CT angiography in the evaluation of acute stroke. AJNR Am J Neuroradiol. 1997; 18: 1011-20.
47. Bagaria SJ, Bagaria VB. Strategies for diagnosis and prevention of venous thromboembolism during pregnancy. J Pregnancy. 2011; 2011: 206858.
48. Sevick-Muraca EM. Translation of near-infrared fluorescence imaging technologies: emerging clinical applications. Annu Rev Med. 2012; 63: 217-31.

49. Krohn M, Ohrndorf S, Werner SG, Schicke B, Burmester GR, Hamm B, et al. Near-infrared Fluorescence Optical Imaging in Early Rheumatoid Arthritis: A Comparison to Magnetic Resonance Imaging and Ultrasonography. J Rheumatol. 2015; 42: 1112-8.
50. Slooter MD, Bierau K, Chan AB, Lowik CW. Near infrared fluorescence imaging for early detection, monitoring and improved intervention of diseases involving the joint. Connect Tissue Res. 2015; 56: 153-60.